Exchange-displacement waves in GdB_6

M. Amara,* S. E. Luca, and R.-M. Galéra
Laboratoire Louis-Néel, C.N.R.S., BP 166X, F-38042 Grenoble, France

F. Givord
DRFMC/SPSMS/MDN, CEA-Grenoble, F-38054 Grenoble, France

C. Detlefs
European Synchrotron Radiation Facility, BP 220, F-38043 Grenoble, France

S. Kunii
Department of Physics, Faculty of Science, Tohoku University, Aramaki, Aoba-ku, Sendai 980, Japan
(Received 13 December 2004; published 26 August 2005)

The antiferromagnetic states of GdB_6 are investigated both theoretically and experimentally. A mean-field model is introduced which predicts the coexistence of magnetic and displacement waves starting from isotropic exchange and magnetic ions in a harmonic potential. It provides a coherent interpretation of the puzzling features of GdB_6 magnetic order, in particular the first-order magnetic transition at T_N and the two successive antiferromagnetic states. X-ray scattering experiments show $\langle \frac{1}{2}\ 0\ 0 \rangle$, $\langle \frac{1}{2}\ \frac{1}{2}\ 0 \rangle$, and $\langle \frac{1}{4}\ \frac{1}{4}\ \frac{1}{2} \rangle$ satellites consistent with displacement waves imposed by the magnetic $\langle \frac{1}{4}\ \frac{1}{4}\ \frac{1}{2} \rangle$ structures. In the high-temperature phase, the observation of second-order displacement reflections is evidence of a multi-q, $\langle \frac{1}{2}\ 0\ 0 \rangle$, displacement structure: a model of magnetic structure, consistent with both the displacement pattern and the mean-field model predictions, is proposed.

DOI: 10.1103/PhysRevB.72.064447 PACS number(s): 75.25.+z, 61.10.−i, 75.40.−s

I. INTRODUCTION

In rare-earth compounds, along with the magnetic degeneracy, additional degrees of freedom related to the charge distribution may influence the nature and thermodynamics of the ordered magnetic states. Such effects are central in the magnetism of systems based on rare-earth ions with total orbital momentum $L \neq 0$. The related orbital degeneracy allows the $4f$ electronic distribution to adapt to the crystal-field symmetry,[1–3] giving rise to magnetic anisotropy. For rare-earth sites of high enough point symmetry, e.g., multiaxial sites, the orbital degeneracy partly survives the crystal field and is involved in the magnetic ordering phenomena. Then, in addition to the magnetic moments, emerge quadrupolar moments, describing a change in the $4f$ asphericity. Due to their own pair interactions and coupling with the lattice, they participate in the minimization of the collective energy. In this secondary order-parameter role, they have been proved to determine the multiaxial nature of magnetic structures, to induce sizable magnetostriction phenomena and, as well as the crystal field, to influence the magnetic transitions in their type (first or second order), temperature, and applied field.[4]

In the case of lack of orbital degeneracy, that is, for magnetic ions with $L=0$, one could expect much simpler features for the magnetic order. Indeed, in most gadolinium compounds, one observes essentially isotropic magnetic properties, negligible magnetoelastic phenomena, and a single magnetic state below a typical second-order Curie or Néel point. There are, however, remarkable exceptions in which the observed properties recall those evoked above for the $L \neq 0$ case. An alternative mechanism, relying on other degrees of freedom than those of the $4f$ orbitals, is then to be invoked. In the case of the GdMg compound and its canted[5] magnetic structure a biquadratic correction to the isotropic exchange, arising from the orbital character of the conduction electrons (rather than the $4f$ shell), has been proposed.[6] Another way for the system to minimize its ordered state energy, by acting on the charge distribution, may be a macroscopic strain reducing the exchange energy. This mechanism of exchange striction has been evoked in the case of $3d$ systems, in particular for explaining the first-order magnetic transitions in MnAs (Ref. 7) and MnO (Ref. 8). This is also the way magnetoelastic phenomena are usually described in $4f$ intermetallic compounds which lack an orbital degeneracy, i.e., in gadolinium systems. However, due to the elastic energy cost of the strain, this magnetoelastic scenario is far from approaching that of a true degeneracy (between the strained and unstrained states of the crystal) and the related effects remain small, if not negligible. To get closer to degeneracy, one would need an underlying lattice instability. This seems to be realized in some $L \neq 0$ systems, simultaneously undergoing a structural and magnetic first-order transformation (see, for instance, the case of TbCu in Ref. 9), but, to the best of our knowledge, there is not such an example among gadolinium compounds. The present paper focuses on a variant of this scenario, in which the instability is expressed by static atomic displacements waves with negligible macroscopic strain. These atomic displacements may be connected with the unusual magnetic order properties of the GdB_6 compound.

This compound crystallizes within the CaB_6-type crystal structure (space group $Pm\bar{3}m$), the rare-earth ion sitting at the center of a cubic cage consisting of eight boron octaedra.

It orders antiferromagnetically[10] at $T_N=15.5$ K, in a first-order process, and a second,[11] again first-order, transition occurs within the magnetic order range at $T^*=8$ K. In favor of the displacement waves scenario are the results of an x-ray-diffraction experiment which shows the emergence of $\langle \frac{1}{2}\ 0\ 0\rangle$ and $\langle \frac{1}{2}\ \frac{1}{2}\ 0\rangle$ charge satellites concomitantly with the antiferromagnetic states.[12] These wave vectors differ from the magnetic $\langle \frac{1}{4}\ \frac{1}{4}\ \frac{1}{2}\rangle$ ones, recently established[13] from powder neutron diffraction. Kasuya pointed out that the change in the charge periodicity, then the emergence of the x-ray satellites, occurs through the coherent displacements of the gadolinium ions inside their boron cages.[14] In his approach, Kasuya considers the effect of a true degeneracy, each rare-earth ion having multiple equilibrium positions inside the cage. At low temperature, the system reduces this degeneracy by moving the magnetic ions in order to decrease its exchange energy by pairing adjacent Gd ions.

In the present paper, a model is introduced which also considers the displacement of the rare-earth ions inside a rigid boron lattice. However, no true position degeneracy is considered, the ions moving in a simple harmonic potential. The displacement in this well results from a compromise between the elastic and exchange energies of the antiferromagnetic state. No special pairing mechanism is then introduced, the movement of any ion resulting from its indirect Ruderman-Kittel-Kasuya-Yosida (RKKY) exchange coupling with an infinite number of neighbors. The model is treated in a simple mean-field approach which allows us to detail the relationship between magnetic and displacement structures. This mean-field treatment is also sufficient for predicting a first-order magnetic transition at T_N.

Thereafter, the results of a series of x-ray-diffraction measurements are presented and their consistency with the model's predictions discussed. On this basis, a magnetic structure is proposed for the GdB_6 high-temperature antiferromagnetic state.

II. EXCHANGE DISPLACEMENT AND MAGNETIC ORDERING

A. Mean-field, harmonic model

We consider an assembly of magnetic ions located on a simple cubic lattice and interacting via Heisenberg exchange. In addition to its magnetic degeneracy, each ion at site i has three space degrees of freedom defining its displacement $\boldsymbol{d}_i$ apart from the cubic lattice site $\boldsymbol{R}_i$. The movement of the ions in their crystal environment has to be accounted for with a specific displacement term $\mathcal{H}_d$ in the system Hamiltonian. The starting point is then a total Hamiltonian including both the usual Heisenberg term and $\mathcal{H}_d$:

$$\mathcal{H}=-\sum_{i\neq j}\mathcal{J}_{ij}\boldsymbol{J}_i\cdot\boldsymbol{J}_j+\mathcal{H}_d, \tag{1}$$

where $\mathcal{J}_{ij}=\mathcal{J}(\boldsymbol{R}_j-\boldsymbol{R}_i)$ is the isotropic coupling constant between the ions at sites i and j, with, respectively, $\boldsymbol{J}_i$ and $\boldsymbol{J}_j$ total momentum. Obviously, $\mathcal{J}_{ij}$ should depend on the ions displacements, which means the Heisenberg and displacement terms in $\mathcal{H}$ are coupled. A number of simplifications are then needed to reduce this initial Hamiltonian to a tractable form.

The displacements remaining extremely small compared to the lattice parameter, a first-order expansion of the coupling $\mathcal{J}_{ij}$ should be adequate within the adiabatic approximation. This is the usual way exchange corrections are accounted for.[7,8,15] Introducing the gradient $\boldsymbol{g}_{ij}=\nabla\mathcal{J}(\boldsymbol{R}_j-\boldsymbol{R}_i)$ (beware of the index sequence as $\boldsymbol{g}_{ij}=-\boldsymbol{g}_{ji}$) of the exchange coupling one thus obtains

$$\mathcal{H}=-\sum_{i\neq j}\mathcal{J}^0_{ij}\boldsymbol{J}_i\cdot\boldsymbol{J}_j-\sum_{i\neq j}[\boldsymbol{g}_{ij}\cdot(\boldsymbol{d}_j-\boldsymbol{d}_i)]\boldsymbol{J}_i\cdot\boldsymbol{J}_j+\mathcal{H}_d, \tag{2}$$

where $\mathcal{J}^0_{ij}$ is the exchange coupling for magnetic ions at their original paramagnetic equilibrium position. The question is now to give a form to the displacement term $\mathcal{H}_d$. It should include the kinetic energy of the ions together with an energy potential. The simplest picture that we may consider is that of magnetic ions interacting with their immediate environment, without consideration of the displacements of the other rare-earth ions. In such conditions, the energy potential reduces to a sum of single ions terms which, to the first order of interest, are a simple, isotropic, quadratic form of the displacement. $\mathcal{H}_d$ then describes a collection of identical harmonic oscillators:

$$\mathcal{H}_d=\sum_{i=1}^{N}-\frac{\hbar^2}{2m}\nabla^2+A^\alpha\boldsymbol{d}_i^2, \tag{3}$$

where A^α defines the harmonic potential recalling the ions to their paramagnetic positions. All variations of A^α will be neglected in the thermal range of our investigations. Focusing on one of these oscillators with displacement $\boldsymbol{d}_i$ and considering the related linear terms in Eq. (2), it appears that, in classical terms, the effect of the exchange coupling is a force exerted on the magnetic ion. Since it involves the product of total momentum operators, this force is a fluctuating one. However, as it results from a sum with numerous terms and, moreover, as it can be expected to fluctuate on time scales much shorter than the period of the oscillator, it is reasonable to consider this force as constant. The effect of this force is then simply to shift the position of minimum energy of the harmonic oscillator by $\langle\boldsymbol{d}_i\rangle$. Thanks to this approximation, the dynamic of the set of harmonic oscillators is decoupled from the magnetic part of the Hamiltonian. For the remainder of this paper, we consider only the mean displacement $\langle\boldsymbol{d}_i\rangle$, which, for simplicity, will be denoted by $\boldsymbol{d}_i$. It interferes in the magnetic part of the Hamiltonian through (mean) changes of the couplings and an elastic energy term. Applying the mean-field approximation to the exchange part, the effective single ion Hamiltonian of site i becomes

$$\mathcal{H}_i=-\boldsymbol{H}_i^m\boldsymbol{J}_i+A^\alpha\boldsymbol{d}_i^2, \tag{4}$$

where $\boldsymbol{H}_i^m$ states for the mean-field acting at site i

$$\boldsymbol{H}_i^m=\sum_{j,j\neq i}[\mathcal{J}^0_{ij}+\boldsymbol{g}_{ij}\cdot(\boldsymbol{d}_j-\boldsymbol{d}_i)]\langle\boldsymbol{J}_j\rangle. \tag{5}$$

The equilibrium value of $\boldsymbol{d}_i$, that is, the shift due to the above evoked force, corresponds to the minimum internal energy, formally $\mathcal{H}_i$, with respect to $\boldsymbol{d}_i$:

$$\boldsymbol{d}_i = -\frac{1}{2A^{\alpha}} \sum_{j,j\neq i} (\langle \boldsymbol{J}_j \rangle \cdot \langle \boldsymbol{J}_i \rangle) \boldsymbol{g}_{ij}. \tag{6}$$

In this way a strict relation is established between the magnetic order and the consequent displacement field. In theory, this relation can be used for solving iteratively the mean-field Hamiltonian of Eq. (4), the values for the magnetic moment and displacement at any site being thus determined at each iteration.

B. Use of fourier analysis

1. Fourier series of the displacements

Defining the displacement at site i after an infinite sum as in Eq. (6) is clearly unpractical. As the magnetic order, the displacement field should develop with well defined periodicities. One may take advantage of this using Fourier analysis starting from the components $\boldsymbol{m}_k$ and wave vectors $\boldsymbol{k}$ defining the magnetic structure,

$$\boldsymbol{m}_i = \langle \boldsymbol{J}_i \rangle = \sum\nolimits_k \boldsymbol{m}_k \exp[j\boldsymbol{k}\boldsymbol{R}_i], \tag{7}$$

where $j^2=-1$. Then, introducing the Fourier transform $\boldsymbol{\Gamma}_k$,

$$\boldsymbol{\Gamma}_k = \sum_{j,j\neq i} \boldsymbol{g}_{ij} \exp[-j\boldsymbol{k}(\boldsymbol{R}_j - \boldsymbol{R}_i)], \tag{8}$$

of the exchange coupling gradient, one may rewrite Eq. (6) as

$$\boldsymbol{d}_i = -\frac{1}{2A^{\alpha}} \sum_{k,k'} (\boldsymbol{m}_k \cdot \boldsymbol{m}_{k'}) \boldsymbol{\Gamma}_{-k} \exp[j(\boldsymbol{k}+\boldsymbol{k}')\boldsymbol{R}_i]. \tag{9}$$

It thus clearly appears that the wave vectors $\boldsymbol{q}$ describing the displacement pattern are all of the form $\boldsymbol{q}=\boldsymbol{k}+\boldsymbol{k}'$ where $\boldsymbol{k}$ and $\boldsymbol{k}'$ are magnetic wave vectors. Note that the dissymmetry between $\boldsymbol{k}$ and $\boldsymbol{k}'$ in Eq. (9) is only apparent since each $(\boldsymbol{k},\boldsymbol{k}')$ term of the sum has a symmetric $(\boldsymbol{k}',\boldsymbol{k})$ counterpart. This equation shows that the polarization of the displacement waves depends entirely on the $\boldsymbol{\Gamma}_k$ vectors, which directions can be specified from symmetry arguments.

2. Polarization of the displacement waves; $\langle \frac{1}{4}\ \frac{1}{4}\ \frac{1}{2} \rangle$ case

a. General case. As it appears in Eq. (9), the atomic displacements are linear combinations of the $\boldsymbol{\Gamma}_k$ vectors. These vectors are the Fourier transform of the exchange coupling gradient $\boldsymbol{g}_{ij}$ which, from a center at a given i site, defines a field of cubic symmetry. As a result, the $\boldsymbol{\Gamma}_k$ vectors should conform to well defined transformation rules. From Eq. (8), it can be easily derived that, for any point symmetry operation of the group (here the cubic group) T, the image of $\boldsymbol{\Gamma}_k$ is

$$T(\boldsymbol{\Gamma}_k) = \boldsymbol{\Gamma}_{T(k)}.$$

This means that $\boldsymbol{\Gamma}_k$ is at least as symmetrical as $\boldsymbol{k}$. Actually, due to the equivalence between $\boldsymbol{k}$ and $\boldsymbol{k}+\boldsymbol{H}$, where $\boldsymbol{H}$ is a reciprocal-lattice translation, the point symmetry group of $\boldsymbol{\Gamma}_k$ can be extended and identifies with the so-called little cogroup of $\boldsymbol{k}$. Indeed, if there exists a cubic transformation T such that $T(\boldsymbol{k})=\boldsymbol{k}+\boldsymbol{H}$, then $T(\boldsymbol{\Gamma}_k)=\boldsymbol{\Gamma}_{k+H}=\boldsymbol{\Gamma}_k$, which means T preserves $\boldsymbol{\Gamma}_k$. Such a situation occurs for wave vectors with at least one-half integer index.

The additional symmetry elements mean additional restrictive conditions on the direction of $\boldsymbol{\Gamma}_k$. In some cases, one can even deduce that $\boldsymbol{\Gamma}_k$ cancels. This happens for magnetic wave vectors which are high-symmetry points of the first zone boundary, such as $\boldsymbol{k}=\left[\frac{1}{2}\ 0\ 0\right]$, as then $-\boldsymbol{k}$ is equivalent to $\boldsymbol{k}$. Considering the inversion symmetry one can deduce $-\boldsymbol{\Gamma}_k=\boldsymbol{\Gamma}_{-k}=\boldsymbol{\Gamma}_k$, which forces $\boldsymbol{\Gamma}_k$ and therefore the displacements to cancel. This result is by no means surprising since only centrosymmetric magnetic structures, inconsistent with displacements, can be described by magnetic wave vectors such as $\boldsymbol{k}=\left[\frac{1}{2}\ 0\ 0\right]$.

b. Application to the $\langle \frac{1}{4}\ \frac{1}{4}\ \frac{1}{2} \rangle$ wave vectors In the less obvious case of the $\langle \frac{1}{4}\ \frac{1}{4}\ \frac{1}{2} \rangle$ magnetic wave vector star of GdB_6, the one-half index allows us to identify an additional symmetry plane for the $\boldsymbol{\Gamma}_k$ vector. For instance, $\boldsymbol{\Gamma}_{\left[\frac{1}{4}\ \frac{1}{4}\ \frac{1}{2}\right]}$ is invariant through the (001) plane. This conservation is due to the reciprocal lattice equivalence between $\left[\frac{1}{4}\ \frac{1}{4}\ \frac{1}{2}\right]$ and $\left[\frac{1}{4}\ \frac{1}{4}\ \bar{\frac{1}{2}}\right]$. The symmetry plane $(1\bar{1}0)$, in which $\left[\frac{1}{4}\ \frac{1}{4}\ \frac{1}{2}\right]$ is invariant, also preserves $\boldsymbol{\Gamma}_{\left[\frac{1}{4}\ \frac{1}{4}\ \frac{1}{2}\right]}$. Being preserved through these two symmetry planes, $\boldsymbol{\Gamma}_{\left[\frac{1}{4}\ \frac{1}{4}\ \frac{1}{2}\right]}$ is necessarily parallel to their intersection, in the present case, the [110] direction. This may be formalized writing

$$\boldsymbol{\Gamma}_{\left[\frac{1}{4}\ \frac{1}{4}\ \frac{1}{2}\right]} = j\frac{G}{\sqrt{2}}[110], \tag{10}$$

where G is a real scalar characterizing the gradient of the coupling for the $\langle \frac{1}{4}\ \frac{1}{4}\ \frac{1}{2} \rangle$ wave-vector star. According to the above transformation rules, this result immediately generalizes to all the $\langle \frac{1}{4}\ \frac{1}{4}\ \frac{1}{2} \rangle$ branches. After Eq. (9) the wave vectors describing the displacements pattern are of the form $\boldsymbol{q}=\boldsymbol{k}+\boldsymbol{k}'$ where $\boldsymbol{k}$ belong here to the $\langle \frac{1}{4}\ \frac{1}{4}\ \frac{1}{2} \rangle$ magnetic wave-vectors star. On this basis one can predict that the displacement wave vectors belong to the stars: $\langle \frac{1}{4}\ \frac{1}{4}\ \frac{1}{2} \rangle$, $\langle \frac{1}{2}\ \frac{1}{2}\ 0 \rangle$, $\langle \frac{1}{4}\ \frac{1}{4}\ 0 \rangle$, and $\langle \frac{1}{2}\ 0\ 0 \rangle$.

The question is then whether the polarization of the displacement waves propagated by theses vectors can be derived from Eq. (10). This first requires us to group the terms in the sum of Eq. (9) which correspond to the same wave vector $\boldsymbol{q}$. Doing this, one obtains the Fourier description of the displacement pattern via the $\boldsymbol{\delta}_q$ components:

$$\boldsymbol{d}_i = \sum\nolimits_q \boldsymbol{\delta}_q \exp[j\boldsymbol{q}\boldsymbol{R}_i]. \tag{11}$$

Representative components, for each one of the displacement wave-vector stars, are listed below:

$$\boldsymbol{\delta}_{\left[\frac{1}{4}\ \frac{1}{4}\ \frac{1}{2}\right]} = j\frac{G}{2\sqrt{2}A^{\alpha}}\{(\boldsymbol{m}_{\left[\bar{\frac{1}{4}}\ \frac{1}{2}\ \frac{1}{4}\right]}\boldsymbol{m}_{\left[\frac{1}{2}\ \bar{\frac{1}{4}}\ \frac{1}{4}\right]} + \boldsymbol{m}_{\left[\bar{\frac{1}{4}}\ \frac{1}{2}\ \bar{\frac{1}{4}}\right]}\boldsymbol{m}_{\left[\frac{1}{2}\ \bar{\frac{1}{4}}\ \bar{\frac{1}{4}}\right]})[\bar{1}\bar{1}0] + (\boldsymbol{m}_{\left[\bar{\frac{1}{4}}\ \frac{1}{2}\ \frac{1}{4}\right]}\boldsymbol{m}_{\left[\frac{1}{2}\ \bar{\frac{1}{4}}\ \frac{1}{4}\right]} - \boldsymbol{m}_{\left[\bar{\frac{1}{4}}\ \frac{1}{2}\ \bar{\frac{1}{4}}\right]}\boldsymbol{m}_{\left[\frac{1}{2}\ \bar{\frac{1}{4}}\ \bar{\frac{1}{4}}\right]})[002]\}, \quad (12a)$$

$$\boldsymbol{\delta}_{\left[\frac{1}{4}\ \frac{1}{4}\ 0\right]} = j\frac{G}{2\sqrt{2}A^{\alpha}}(\boldsymbol{m}_{\left[\bar{\frac{1}{4}}\ \frac{1}{2}\ \bar{\frac{1}{4}}\right]}\boldsymbol{m}_{\left[\frac{1}{2}\ \bar{\frac{1}{4}}\ \frac{1}{4}\right]} + \boldsymbol{m}_{\left[\bar{\frac{1}{4}}\ \frac{1}{2}\ \frac{1}{4}\right]}\boldsymbol{m}_{\left[\frac{1}{2}\ \bar{\frac{1}{4}}\ \bar{\frac{1}{4}}\right]})[\bar{1}\bar{1}0], \quad (12b)$$

$$\boldsymbol{\delta}_{\left[\frac{1}{2}\ \frac{1}{2}\ 0\right]} = j\frac{G}{2\sqrt{2}A^{\alpha}}\{(\boldsymbol{m}^2_{\left[\frac{1}{4}\ \frac{1}{4}\ \frac{1}{2}\right]} - \boldsymbol{m}^2_{\left[\bar{\frac{1}{4}}\ \bar{\frac{1}{4}}\ \frac{1}{2}\right]})[110] + (\boldsymbol{m}^2_{\left[\frac{1}{4}\ \bar{\frac{1}{4}}\ \frac{1}{2}\right]} - \boldsymbol{m}^2_{\left[\bar{\frac{1}{4}}\ \frac{1}{4}\ \frac{1}{2}\right]})[1\bar{1}0]\}, \quad (12c)$$

$$\boldsymbol{\delta}_{\left[\frac{1}{2}\ 0\ 0\right]} = j\frac{G}{\sqrt{2}A^{\alpha}}(\boldsymbol{m}_{\left[\frac{1}{4}\ \frac{1}{4}\ \frac{1}{2}\right]}\boldsymbol{m}_{\left[\frac{1}{4}\ \bar{\frac{1}{4}}\ \frac{1}{2}\right]} - \boldsymbol{m}_{\left[\bar{\frac{1}{4}}\ \bar{\frac{1}{4}}\ \frac{1}{2}\right]}\boldsymbol{m}_{\left[\bar{\frac{1}{4}}\ \frac{1}{4}\ \frac{1}{2}\right]} + \boldsymbol{m}_{\left[\frac{1}{4}\ \frac{1}{2}\ \frac{1}{4}\right]}\boldsymbol{m}_{\left[\frac{1}{4}\ \frac{1}{2}\ \bar{\frac{1}{4}}\right]} - \boldsymbol{m}_{\left[\bar{\frac{1}{4}}\ \frac{1}{2}\ \bar{\frac{1}{4}}\right]}\boldsymbol{m}_{\left[\bar{\frac{1}{4}}\ \frac{1}{2}\ \frac{1}{4}\right]}) \times [100]. \quad (12d)$$

The displacements waves propagated by $\langle \frac{1}{2}\ 0\ 0 \rangle$ or $\langle \frac{1}{4}\ \frac{1}{4}\ 0 \rangle$ vectors are so predicted to be longitudinal, whereas the $\langle \frac{1}{4}\ \frac{1}{4}\ \frac{1}{2} \rangle$ and $\langle \frac{1}{2}\ \frac{1}{2}\ 0 \rangle$ cases appear more intricate. Some simplification may be obtained if one considers some restriction on the magnetic structure. In rare-earth systems where all the magnetic sites are equivalent, one expects the magnetic order to favor structures in which the magnetic moments amplitude is constant, their direction being imposed by the anisotropy. Obviously, for a S ion system the anisotropy is less relevant but the condition of the constant (and maximum) amplitude holds since it tends to minimize the exchange energy. Expressing this condition for the magnetic structure results in not less than 30 equations corresponding to the cancellation, out of the zone center, of all the Fourier components of the squared magnetic moment. Using these relations, one can simplify the expressions of the displacement Fourier components of Eqs. (12) thus obtaining

$$\boldsymbol{\delta}_{\left[\frac{1}{4}\ \frac{1}{4}\ \frac{1}{2}\right]} = j\frac{\sqrt{2}G}{A^{\alpha}}(\boldsymbol{m}_{\left[\bar{\frac{1}{4}}\ \frac{1}{2}\ \frac{1}{4}\right]}\boldsymbol{m}_{\left[\frac{1}{2}\ \bar{\frac{1}{4}}\ \frac{1}{4}\right]})[001], \quad (13a)$$

$$\boldsymbol{\delta}_{\left[\frac{1}{4}\ \frac{1}{4}\ 0\right]} = [000], \quad (13b)$$

$$\boldsymbol{\delta}_{\left[\frac{1}{2}\ \frac{1}{2}\ 0\right]} = j\frac{G}{2\sqrt{2}A^{\alpha}}\{(\boldsymbol{m}^2_{\left[\frac{1}{4}\ \frac{1}{4}\ \frac{1}{2}\right]} - \boldsymbol{m}^2_{\left[\bar{\frac{1}{4}}\ \bar{\frac{1}{4}}\ \frac{1}{2}\right]})[110] + (\boldsymbol{m}^2_{\left[\frac{1}{4}\ \bar{\frac{1}{4}}\ \frac{1}{2}\right]} - \boldsymbol{m}^2_{\left[\bar{\frac{1}{4}}\ \frac{1}{4}\ \frac{1}{2}\right]})[1\bar{1}0]\}, \quad (13c)$$

$$\boldsymbol{\delta}_{\left[\frac{1}{2}\ 0\ 0\right]} = j\frac{\sqrt{2}G}{A^{\alpha}}(\boldsymbol{m}_{\left[\frac{1}{4}\ \frac{1}{4}\ \frac{1}{2}\right]}\boldsymbol{m}_{\left[\frac{1}{4}\ \bar{\frac{1}{4}}\ \frac{1}{2}\right]} + \boldsymbol{m}_{\left[\frac{1}{4}\ \frac{1}{2}\ \frac{1}{4}\right]}\boldsymbol{m}_{\left[\frac{1}{4}\ \frac{1}{2}\ \bar{\frac{1}{4}}\right]})[100]. \quad (13d)$$

In the case of a constant amplitude magnetic structure, the polarization of a $\langle \frac{1}{4}\ \frac{1}{4}\ \frac{1}{2} \rangle$ displacement wave is expected to be along the one-half index direction whereas no displacement should occur for $\langle \frac{1}{4}\ \frac{1}{4}\ 0 \rangle$ wave vectors. The longitudinal polarization for $\langle \frac{1}{2}\ 0\ 0 \rangle$ displacement waves is obviously maintained and, for the $\langle \frac{1}{2}\ \frac{1}{2}\ 0 \rangle$ waves, no direction is privileged inside the basal plane of the associated quadratic cell.

C. Influence of the displacements on the magnetic order

1. Factorization of the mean-field

The relation of Eq. (6), which gives the displacement as a result of the magnetic state, may be used to reduce the mean-field Hamiltonian of Eq. (4) to magnetic variables only. This results in the interference of fourth-order magnetic terms in the system energy, then in an influence of the displacements on the order of the magnetic transitions. Unfortunately, the form that is thus obtained is extremely intricate, mixing biquadratic pair and triplet interaction terms. To avoid this complexity, the discussion is here centered on the enhancement of the exchange coupling by the displacements.

In the context of Fourier analysis, the mean field for a magnetic structure involving a single star of wave vectors can be put in the form of a single-site expression. Indeed, in the absence of displacement the exchange term of Eq. (1) results, at any site i, in a mean-field

$$\boldsymbol{H}_i^m = J^0(\boldsymbol{k})\boldsymbol{m}_i, \quad (14)$$

where

$$J^0(\boldsymbol{k}) = \sum_{j,j\neq i} \mathcal{J}_{ij}^0 \exp[-j\boldsymbol{k}(\boldsymbol{R}_j - \boldsymbol{R}_i)] \quad (15)$$

is the unperturbed Fourier transform of the exchange coupling for any of the $\boldsymbol{k}$ vector belonging to the magnetic wave-vector star. In such conditions the mean-field equations are identical for all sites, which means constant amplitude magnetic structures are stabilized. Now, if one accounts for the effect of the displacements on the couplings [as in Eq. (5)], this Fourier transform becomes not only $\boldsymbol{k}$ but also site (i) dependent:

$$J_i(\boldsymbol{k}) = J^0(\boldsymbol{k}) + \sum_{\boldsymbol{q}} \{\boldsymbol{\delta}_{\boldsymbol{q}} \cdot (\boldsymbol{\Gamma}_{\boldsymbol{k}-\boldsymbol{q}} - \boldsymbol{\Gamma}_{\boldsymbol{k}})\} \exp[j\boldsymbol{q}\boldsymbol{R}_i]. \quad (16)$$

The displacements waves do then modulate $J(\boldsymbol{k})$ from site to site, which means the correction does not systematically re-

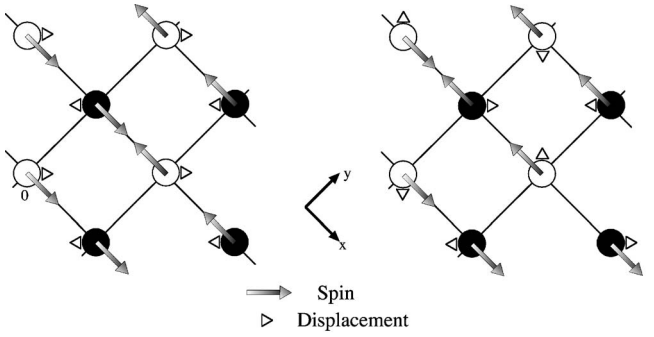

FIG. 1. Planar models of magnetic structures as privileged by the displacement mechanism. The open or black circles refer, respectively, to the sites of nonzero cosine or sine magnetic Fourier components. The magnetic (m) and displacement (δ) Fourier components are listed below the figure. The fourfold direction of the spins, as the (positive) sign for G, are here arbitrary, unlike the twofold directions of the displacements.

sult in an overall reinforced exchange coupling. To minimize its exchange energy, the system adopts an appropriate magnetic structure, which associated displacement scheme maximizes the coupling for all sites. This means that the favored structures are such that the mean field including the displacement correction

$$\boldsymbol{H}_i^m = J^0(\boldsymbol{k})\boldsymbol{m}_i - \sum_{\boldsymbol{q},\boldsymbol{k}} \{\boldsymbol{\delta}_{\boldsymbol{q}} \cdot (\boldsymbol{\Gamma}_{\boldsymbol{q}+\boldsymbol{k}} - \boldsymbol{\Gamma}_{\boldsymbol{k}})\}\boldsymbol{m}_{\boldsymbol{k}} \exp[j(\boldsymbol{q}+\boldsymbol{k})\boldsymbol{R}_i], \tag{17}$$

can be reduced to the simpler form of Eq. (14) with an effective, reinforced, coupling constant that replaces $J^0(\boldsymbol{k})$. These special cases of constant amplitude magnetic structures are then to be identified. This is not an easy task considering the not less than 12 Fourier components describing the general magnetic structure. In order to reduce the difficulty, the discussion hereafter is restricted to magnetic structures based on a reduced set of wave vectors with common one-half index: $\{\boldsymbol{k}_1=\left[\frac{1}{4}\ \frac{1}{4}\ \frac{1}{2}\right],\ \boldsymbol{k}_2=\left[\frac{1}{4}\ \frac{\bar{1}}{4}\ \frac{1}{2}\right],\ \boldsymbol{k}_3=\left[\frac{\bar{1}}{4}\ \frac{1}{4}\ \frac{1}{2}\right],\ \boldsymbol{k}_4=\left[\frac{\bar{1}}{4}\ \frac{1}{4}\ \frac{1}{2}\right]\}$. This four-components situation is obviously easier to handle than the full 12 components one, with the benefits of the following:

(i) A simple planar scheme for the magnetic structures. Indeed, to be consistent with GdB_6 powder neutron diffraction results,[13] the magnetic moments are in the basal plane (001).

(ii) A drastically simplified magnetic picture when using a cosine and sine Fourier description; within the (001) plane, the sites can be separated in two interlaced square lattices (see Fig. 1), one for the sines (full black circles) the other for the cosines (open circles). As a result, one can consider two separate magnetic structures, each based on two components, instead of an intricate four-component one. Moreover, the two sine (respectively, cosine) components need to be perpendicular in order to obey the constant amplitude condition.

(iii) An associated set of possible charge wave vectors, after Eqs. (13), $\{\left[\frac{1}{2}\ \frac{1}{2}\ 0\right],\ \left[\frac{1}{2}\ 0\ 0\right],\ \left[0\ \frac{1}{2}\ 0\right]\}$, consistent with the charge periodicities reported in Ref. 12.

(iv) A basis for building models with up to 12 components by combining two or three planar solutions, although the obtained set of structures cannot be considered as exhaustive.

The point is now to find the conditions on the magnetic components under which the mean field factorizes. The mean-field corrective term appearing in Eq. (17),

$$d\boldsymbol{H}_i^m = -\sum_{\boldsymbol{q},\boldsymbol{k}} \{\boldsymbol{\delta}_{\boldsymbol{q}} \cdot (\boldsymbol{\Gamma}_{\boldsymbol{q}+\boldsymbol{k}} - \boldsymbol{\Gamma}_{\boldsymbol{k}})\}\boldsymbol{m}_{\boldsymbol{k}} \exp[j(\boldsymbol{q}+\boldsymbol{k})\boldsymbol{R}_i],$$

has then to be put in the form of a simple proportion of the local magnetic moment. This requires the four Fourier components of the mean-field correction to be proportional, through the same factor, to their corresponding (i.e., with identical wave vector) magnetic component. This proportionality stands for the cosine and sine components that will be used from now on. The magnetic components describing the structure in terms of sine and cosine waves are defined as

$$\boldsymbol{m}_{1c} = \boldsymbol{m}\left[\frac{1}{4}\ \frac{1}{4}\ \frac{1}{2}\right]_c = \boldsymbol{m}\left[\frac{1}{4}\ \frac{1}{4}\ \frac{1}{2}\right] + \boldsymbol{m}\left[\frac{\bar{1}}{4}\ \frac{\bar{1}}{4}\ \frac{1}{2}\right],$$

$$\boldsymbol{m}_{2c} = \boldsymbol{m}\left[\frac{1}{4}\ \frac{\bar{1}}{4}\ \frac{1}{2}\right]_c = \boldsymbol{m}\left[\frac{1}{4}\ \frac{\bar{1}}{4}\ \frac{1}{2}\right] + \boldsymbol{m}\left[\frac{\bar{1}}{4}\ \frac{1}{4}\ \frac{1}{2}\right],$$

$$\boldsymbol{m}_{1s} = \boldsymbol{m}\left[\frac{1}{4}\ \frac{1}{4}\ \frac{1}{2}\right]_s = j\left(\boldsymbol{m}\left[\frac{1}{4}\ \frac{1}{4}\ \frac{1}{2}\right] - \boldsymbol{m}\left[\frac{\bar{1}}{4}\ \frac{\bar{1}}{4}\ \frac{1}{2}\right]\right),$$

$$\boldsymbol{m}_{2s} = \boldsymbol{m}\left[\frac{1}{4}\ \frac{\bar{1}}{4}\ \frac{1}{2}\right]_s = j\left(\boldsymbol{m}\left[\frac{1}{4}\ \frac{\bar{1}}{4}\ \frac{1}{2}\right] - \boldsymbol{m}\left[\frac{\bar{1}}{4}\ \frac{1}{4}\ \frac{1}{2}\right]\right),$$

where the subscripts c and s, respectively, stand for the cosine and sine components, and the subscripts 1 and 2, respectively, refer to the wave vectors $\boldsymbol{k}_1=\left[\frac{1}{4}\ \frac{1}{4}\ \frac{1}{2}\right]$ and $\boldsymbol{k}_2=\left[\frac{1}{4}\ \frac{\bar{1}}{4}\ \frac{1}{2}\right]$.

Taking advantage of Eqs. (13), in order to replace the displacements components with magnetic ones, the expressions for the mean-field correction components are then

$$d\boldsymbol{H}_{1c}^m = \frac{G^2}{A^\alpha}\{(\boldsymbol{m}_{1c}\boldsymbol{m}_{1s})\boldsymbol{m}_{1s} + (\boldsymbol{m}_{1c}\boldsymbol{m}_{2s})\boldsymbol{m}_{2s}\},$$

$$d\boldsymbol{H}_{2c}^m = \frac{G^2}{A^\alpha}\{(\boldsymbol{m}_{1s}\boldsymbol{m}_{2c})\boldsymbol{m}_{1s} + (\boldsymbol{m}_{2c}\boldsymbol{m}_{2s})\boldsymbol{m}_{2s}\},$$

$$d\boldsymbol{H}_{1s}^m = \frac{G^2}{A^\alpha}\{(\boldsymbol{m}_{1c}\boldsymbol{m}_{1s})\boldsymbol{m}_{1c} + (\boldsymbol{m}_{1s}\boldsymbol{m}_{2c})\boldsymbol{m}_{2c}\},$$

$$d\boldsymbol{H}_{2s}^{m} = \frac{G^2}{A^{\alpha}}\{(\boldsymbol{m}_{1c}\boldsymbol{m}_{2s})\boldsymbol{m}_{1c} + (\boldsymbol{m}_{2c}\boldsymbol{m}_{2s})\boldsymbol{m}_{2c}\}.$$

Factorizing the mean-field correction requires each of its component to obey the proportionality

$$d\boldsymbol{H}_{na}^{m} = \gamma\,\boldsymbol{m}_{na},$$

where n stands for 1 or 2, a stands for c or s, and γ is the scalar characterizing the exchange reinforcement that is to be determined. These equations show that, with the emergence of displacements, a coupling develops between the cosine and sine parts of the magnetic structure. It also appears that there cannot exist a stable mean-field solution if only one, among the four components, cancels. For instance, if $\boldsymbol{m}_{1s}$ is zero, $d\boldsymbol{H}_{2c}^{m}$ and $d\boldsymbol{H}_{1c}^{m}$ are parallel. This means that $\boldsymbol{m}_{2cs}$ and $\boldsymbol{m}_{1c}$ are also parallel, which prevents the constant amplitude for the magnetic moment. This contradiction is, however, solved if $\boldsymbol{m}_{2c}$ cancels together with $\boldsymbol{m}_{1s}$. Then, $\boldsymbol{m}_{1c}$ is parallel with $\boldsymbol{m}_{2s}$ and the magnetic structure reduces to a collinear scheme. Constant amplitude solutions should then consist of two, one cosine and one sine, or of the total four components.

The above four equations also result in four definitions for γ:

$$\gamma = \frac{G^2}{A^{\alpha}}\{(\boldsymbol{u}_{1c}\boldsymbol{m}_{1s})^2 + (\boldsymbol{u}_{1c}\boldsymbol{m}_{2s})^2\},$$

$$\gamma = \frac{G^2}{A^{\alpha}}\{(\boldsymbol{u}_{2c}\boldsymbol{m}_{1s})^2 + (\boldsymbol{u}_{2c}\boldsymbol{m}_{2s})^2\},$$

$$\gamma = \frac{G^2}{A^{\alpha}}\{(\boldsymbol{u}_{1s}\boldsymbol{m}_{1c})^2 + (\boldsymbol{u}_{1s}\boldsymbol{m}_{2c})^2\},$$

$$\gamma = \frac{G^2}{A^{\alpha}}\{(\boldsymbol{u}_{2s}\boldsymbol{m}_{1c})^2 + (\boldsymbol{u}_{2s}\boldsymbol{m}_{2c})^2\},$$

where $\boldsymbol{u}_{na}$ refers to the unitary vector associated with $\boldsymbol{m}_{na}$. The sets $\{\boldsymbol{u}_{1c},\boldsymbol{u}_{2c}\}$ and $\{\boldsymbol{u}_{1s},\boldsymbol{u}_{2s}\}$ do then represent two orthonormal bases of the plane that contains the magnetic moments. Summing the first (or last) two equations yields the expression of γ:

$$\gamma = \frac{G^2}{2A^{\alpha}}m^2.$$

This result is valid for the four-component case only. If two components cancel, two equations are left which both yield

$$\gamma = \frac{G^2}{A^{\alpha}}m^2.$$

It thus clearly appears that the displacements will favor a two-component, collinear, arrangement: the gain in exchange coupling is then twice that of the four-component situation. As a result, the corrected mean field can be written as

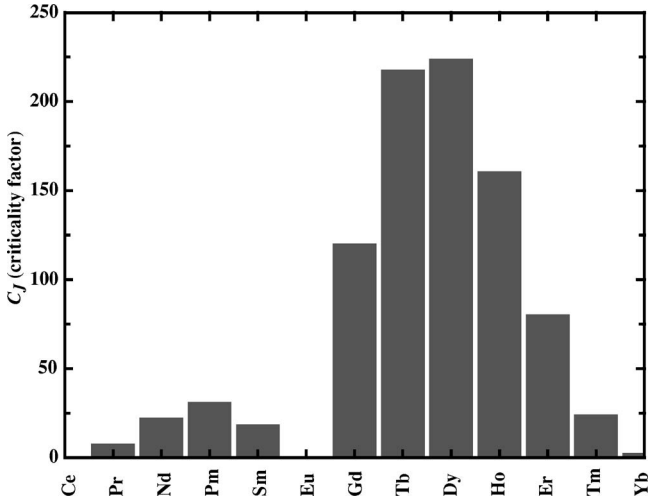

FIG. 2. Evolution for the rare-earth tripositive ions of the criticality factor C_J (see text) which reflects the tendency to order in a first-order process as well as the 0-K displacement amplitude.

$$\boldsymbol{H}_{i}^{m} = \left(J^0(\boldsymbol{k}) + \frac{G^2}{A^{\alpha}}m^2\right)\boldsymbol{m}_i. \tag{18}$$

The two models of magnetic structure which are consistent with this exchange enhancement are represented in Fig. 1, together with their displacement counterparts. One should be aware that, in absence of a defined anisotropy, any spin direction within the plane is acceptable for these uniaxial magnetic structures. Whatever the spin's direction is, the associated displacement structure is completely determined: in both cases the rare-earth ions move along twofold axes, structure (a) being a uniaxial, single-q, $\langle \frac{1}{2}\ \frac{1}{2}\ 0\rangle$, whereas (b) is a biaxial, double-q, $\langle \frac{1}{2}\ 0\ 0\rangle$. Note that combining two or three of such planar solutions in order to build a three-dimensional (3D) model of identical energy is not consistent with these twofold displacement axes. Keeping the energy constant requires that the superimposed solutions do not interfere with each other, thus preserving the single-site description. This is obtained only if the two or three spin directions are orthogonal as well as the displacement directions. The requirement of the orthogonality is easy to fulfill for the spins, due to the lack of anisotropy, but clearly not for the displacements. Indeed, orthogonal twofold axes are found only inside the same plane, for instance, [1 1 0] and [1 −1 0] inside the (0 0 1) plane, which brings the question back to the fully planar approach. At this point, the two collinear magnetic models of Fig. 1 are then our only candidates for a minimum energy of the ordered state.

2. Criticality at T_N

Thanks to the above mean-field factorization, the change of the transition order at T_N, from second to first order, can be most easily interpreted. The only amendment, with respect to the very classical mean-field magnetic problem, is that the function describing the exchange interaction is no longer a straight line but is slightly curved due to the interference of a cubic term in Eq. (18). Consequently, while decreasing the temperature, its intersection with the magnetic

ionic response, here considered of the Brillouin type, can occur for a nonzero value of the magnetic moment. In this event, the transition is first order and develops at a temperature higher than expected in the second-order case. The mathematical criterion, for defining the change from second- to first-order type, is simply the identity of the two-function curvatures, exchange and Brillouin, close to zero magnetic moment at T_N. One can reverse the mean-field expression of Eq. (18) through an expansion of the magnetic moment in odd powers of the field and identify the cubic term with the one of the Brillouin expansion (the one of the third-order susceptibility). This yields the critical identity

$$\frac{G^2}{A^\alpha} = \frac{3}{10}\frac{2J^2+2J+1}{[J(J+1)]^2} J^0(\boldsymbol{k}). \tag{19}$$

A value of G^2/A^α exceeding the right term would then result in a first-order process at T_N. Within the rare-earth hexaboride series, it seems reasonable to consider that the A^α value defining the harmonic potential, then the rare-earth close environment, will not drastically vary. Assuming it as constant and applying the de Gennes scaling[16] to $J^0(\boldsymbol{k})$ and G^2 (G, the amplitude of the Fourier transform of the gradient of the exchange coupling, also obeys the de Gennes law), one can define a parameter C_J representative of the system tendency to order in a first-order process:

$$C_J = \frac{(g_J-1)^2[J(J+1)]^3}{2J(J+1)+1}. \tag{20}$$

It turns out that C_J is also a good approximation of the 0-K, maximum, displacement amplitude [see Eq. (6)].

Figure 2 shows the evolution of C_J across a series. The scaling does not allow us to predict the order of the transition at T_N, but helps us understand the contrast between the elements of the series. Indeed, the striking feature of this diagram is the contrast between heavy and light rare earths; for the latter little influence of exchange displacements can be expected. The harmonic model of the exchange displacement considered here apparently would not help in the controversial[17,18] case of CeB_6. On the contrary, considering Fig. 2, one can predict that exchange displacement waves are very influential at least in TbB_6, DyB_6, and HoB_6. Indeed, as one would extrapolate from the GdB_6 case, these other $\langle \frac{1}{4}\ \frac{1}{4}\ \frac{1}{2} \rangle$ antiferromagnets also order in a first-order process.[13,19,20] However, it has to be reminded that for such $L \neq 0$ ions, orbital effects, which we did not consider here, should also take part in defining the ordered states and the order of the transition at T_N. To this respect, the case of DyB_6 might be the most eloquent, the first-order transformation being reported as nonmagnetic, but ferroquadrupolar.

III. X-RAY-DIFFRACTION INVESTIGATION

A. Diffraction by an atomic displacement wave

The model of the scattering given here corresponds to the most simple picture of the displacement wave. The only displacements that will be considered are those of the rare-earth ions; all changes affecting the lattice of the boron octaedra will be neglected.

In the structure factor, describing the charge x-ray reflections emerging with the development of the displacement wave, only the rare-earth lattice needs to be considered. Obviously, one has also to account for the fact that any site i is no longer located at $\boldsymbol{R}_i$ but at a slightly different $\boldsymbol{R}_i+\boldsymbol{d}_i$. For a scattering vector $\boldsymbol{Q}$, the structure factor $F(\boldsymbol{Q})$ normalized to the primitive lattice cell is then

$$F(\boldsymbol{Q}) = \frac{1}{N}\sum_{i=1}^{N} f_R(Q)\exp[j\boldsymbol{Q}(\boldsymbol{R}_i+\boldsymbol{d}_i)],$$

where N is the number of rare-earth sites inside the displacement cell and $f_R(Q)$ states for the rare-earth (presently Gd) tripositive ion scattering factor. Expanding the exponential term related to $\boldsymbol{d}_i$ gives

$$F(\boldsymbol{Q}) = F_0(\boldsymbol{Q}) + F_1(\boldsymbol{Q}) + F_2(\boldsymbol{Q}) + \cdots \tag{21}$$

with

$$F_0(\boldsymbol{Q}) = \frac{f_R(Q)}{N}\sum_{i=1}^{N} \exp[j\boldsymbol{Q}\boldsymbol{R}_i],$$

$$F_1(\boldsymbol{Q}) = \frac{jf_R(Q)}{N}\sum_{i=1}^{N} (\boldsymbol{Q}\boldsymbol{d}_i)\exp[j\boldsymbol{Q}\boldsymbol{R}_i],$$

$$F_2(\boldsymbol{Q}) = -\frac{f_R(Q)}{2N}\sum_{i=1}^{N} (\boldsymbol{Q}\boldsymbol{d}_i)^2\exp[j\boldsymbol{Q}\boldsymbol{R}_i],$$

where $F_0(\boldsymbol{Q})$ is a structure factor reflecting an unaffected periodicity. It should be composed with the equivalent scattering term from the boron octaedra, thus defining the structure factor for the primitive lattice reflections.

Much more interesting is the first-order structure factor $F_1(\boldsymbol{Q})$ which reflects the periodicity of the displacement wave through $(\boldsymbol{Q}\boldsymbol{d}_i)$ and that is the main contributor to satellite reflections. These reflections then display a characteristic dependence on the scattering angle; the intensity cancels toward zero angle, is maximum at intermediate scattering angles, and decreases at higher angles due to the ionic form factor $f_R(Q)$. In addition, as a scalar product between the scattering vector $\boldsymbol{Q}$ and the displacement $\boldsymbol{d}_i$ is involved, the intensity of the reflections should give information on the polarization of the displacement wave. The second-order term $F_2(\boldsymbol{Q})$ will reflect the periodicities of $(\boldsymbol{Q}\boldsymbol{d}_i)^2$ which are obviously not the ones of $(\boldsymbol{Q}\boldsymbol{d}_i)$. It may contribute to the primitive lattice reflections in the case, for instance, of a collinear antiphase displacement wave. However, in general, they will be responsible for the emergence of additional charge satellites at reciprocal space nodes distinct from the first-order ones. Due to the interference of $\boldsymbol{Q}^2$, their scattering angle dependence should impede them from being confused with first-order satellites. In particular, the maximum of the intensity will occur at much larger angles than in the first-order case. One could as well discuss the third-order case. However, the higher the order the lower will be the intensity of the related satellites, then the probability of a reliable observation.

As many wave vectors may be involved in the description of $\boldsymbol{d}_i$ (see Sec. II B 1), with as many related elementary cells defining the set of N atoms, it appears much more convenient to use Fourier series for writing the structure factors. Starting from the Fourier series of the displacement [Eq. (11)], the first- and second-order structure factors become

$$F_1(\boldsymbol{Q}) = \frac{jf_R(Q)}{N} \sum_q (\boldsymbol{Q}\boldsymbol{\delta}_q) \sum_{i=1}^{N} \exp[j(\boldsymbol{Q}+\boldsymbol{q})\boldsymbol{R}_i],$$

$$F_2(\boldsymbol{Q}) = -\frac{f_R(Q)}{2N} \sum_{q,q'} (\boldsymbol{Q}\boldsymbol{\delta}_q)(\boldsymbol{Q}\boldsymbol{\delta}_{q'}) \sum_{i=1}^{N} \exp[j(\boldsymbol{Q}+\boldsymbol{q}+\boldsymbol{q}')\boldsymbol{R}_i].$$

A first-order reflection will occur if the scattering vector $\boldsymbol{Q}$ is such that $\boldsymbol{Q}+\boldsymbol{q}=\boldsymbol{H}$, where $\boldsymbol{q}$ is a displacement wave vector and $\boldsymbol{H}$ is a node of the primitive reciprocal lattice. Neglecting the possible interference with higher orders of scattering, the collected intensity is then described by the structure factor

$$F_1(\boldsymbol{Q}) = jf_R(Q)\boldsymbol{Q}\boldsymbol{\delta}_q. \tag{22}$$

The second-order reflections will be observed for scattering vectors $\boldsymbol{Q}$ such that $\boldsymbol{Q}+\boldsymbol{q}+\boldsymbol{q}'=\boldsymbol{H}$, where $\boldsymbol{q}$ and $\boldsymbol{q}'$ are two displacement wave vectors. In this case the collected intensity will be described by the structure factor

$$F_2(\boldsymbol{Q}) = -\frac{f_R(Q)}{2} \sum_{q+q'=H-Q} (\boldsymbol{Q}\boldsymbol{\delta}_q)(\boldsymbol{Q}\boldsymbol{\delta}_{q'}), \tag{23}$$

where the sum collects all terms such that $\boldsymbol{Q}+\boldsymbol{q}+\boldsymbol{q}'=\boldsymbol{H}$.

All of the above equations refer to a crystal whose entire volume is described by a unique displacement structure. Except for a cubic displacement structure, this is unlikely to happen and one has to confront the question of the domains. The intensity of a displacement Bragg reflection has then to be considered as the addition of the contributions of several domains. The simplest way to account for the interference of domains in the experimental intensity is to consider a single-q, collinear, displacement structure and its associated domains volume fractions. With little adjustments, the form of theoretical intensity, structure factor, that is thus obtained also applies in case of a multiaxial structure. After Eq. (22), for a displacement wave of constant amplitude δ, the first-order structure factor describing the experimental data takes the form

$$F_{\mathrm{cal}}(\boldsymbol{Q}) = f_R(Q)Q\delta D(\boldsymbol{Q}), \tag{24}$$

where the $D(\boldsymbol{Q})$ factor accounts for the domain distribution. In the case of a collinear displacement wave considered here

$$D(\boldsymbol{Q}) = \sqrt{\frac{1}{n}\sum_i v_i \cos^2\alpha_i} = \sqrt{\frac{v_q}{n}\langle\cos^2\alpha\rangle}, \tag{25}$$

where the index i refers to one of the domains with wave vector $\boldsymbol{q}$ complying with the scattering condition, with an angle α_i between $\boldsymbol{Q}$ and $\boldsymbol{\delta}_i$, and with volume fraction v_i. In the alternative form of the right member, the squared cosine is already averaged and the volume fraction v_q is the sum of all the v_i. The n divisor is not related to domains but is there for dealing with both of these situations:

(i) $\boldsymbol{q}$ is equivalent to $-\boldsymbol{q}$, in which case $n=1$ ($\langle \frac{1}{2}\ \frac{1}{2}\ 0\rangle$ or $\langle \frac{1}{2}\ 0\ 0\rangle$ cases);

(ii) $\boldsymbol{q}$ is not equivalent to $-\boldsymbol{q}$, in which case $n=2$ as the scattered intensity divides into two satellite reflections ($\langle \frac{1}{4}\ \frac{1}{4}\ 0\rangle$ or $\langle \frac{1}{4}\ \frac{1}{4}\ \frac{1}{2}\rangle$ cases).

To build high-symmetry, multiaxial, displacement structures from collinear models, one can associate symmetry equivalent waves with perpendicular polarizations in order to keep a constant amplitude. The number of domains is then reduced, down to 1 in the case of a structure preserving the cubic symmetry. Thus the volume of crystal contributing to a particular reflection increases whereas, for a fixed total displacement amplitude, the individual amplitude of the waves decreases. However, the form of Eq. (24) can still be used to reproduce an experiment; if one considers that δ represents the total displacement, the reduction of the individual wave's amplitude has to be transferred to the $D(\boldsymbol{Q})$ factor. In the situation of domain equipartition, this reduction exactly compensates the increase in the volume fraction. The $D(\boldsymbol{Q})$ factor, as $F_{\mathrm{cal}}(\boldsymbol{Q})$, is then the same for a single-q or a multi-q displacement structure and the measured intensity only reflects the total amplitude of the displacement.

B. X-ray-diffraction experiments

The experiments have been performed at the ESRF on the ID20 beamline. The use of an "orange" ILL-type cryostat has imposed a horizontal diffraction plane and a π incident polarization. No polarization analysis of the diffracted beam was performed. In order to explore a wide range of the reciprocal space an incident energy of 18 keV ($\lambda=0.6886$ Å) was selected [the room-temperature lattice parameter of GdB_6 is $a=4.111$ Å (Ref. 21)]. This rather high energy also ensures that the penetration depth, then the sample's volume contributing to the scattering, is large. In addition, it is far enough from x-ray-absorption edges of both the Gd and B, which means reduced noise levels are expected.

The incident beam was collimated to obtain a spot of 0.5×0.5 mm^2 at the sample surface. This sample is the same single crystalline plate, 4×4 mm^2 (1 mm thick) cut along the (1 1 0) surface as the one used in the experiments reported in Ref. 12. For the present experiments, it was oriented so that the [1 1 0] axis perpendicular to the largest surface (specular direction) and the [0 0 1] axis parallel to this surface define the horizontal diffraction plane. The sample was lined up at 1.7 K, the lowest reachable temperature, using the main reflections of the CaB_6 structure of the type (h h l) and (h h 0). It appeared somewhat difficult to build a satisfactory orientation matrix from these reflections. In particular, integrated intensities obtained from ω scans around symmetric, (h h l) and (h h $-l$), off-specular reflections showed up to 50% dispersion. This appeared to be due to the mosaic spread of the crystal (about 0.02 °) combined with a high instrumental resolution and a small beam size: the (h h l) and (h h $-l$) reflections came from slightly misaligned areas of the sample, more or less consistent with the orientation matrix. However, this matrix was accurate for the specular reflections and was also used elsewhere, for a first

TABLE I. $T=1.7$ K, x-ray satellites associated with the $\left[\frac{1}{2}\ \frac{1}{2}\ 0\right]$ displacement wave vector. Columns 2 and 3 show the experimental F_{exp} and calculated, F_{cal}, structure factors. F_{cal} is calculated for a relative displacement amplitude $\delta_{\langle \frac{1}{2}\ \frac{1}{2}\ 0\rangle}/a=8.8\times10^{-4}$, assuming domains equipartition.

$(h\ k\ l)$			$F_{exp}(10^{-3}\ e^-)$	$F_{cal}(10^{-3}\ e^-)$
1/2	1/2	0	51±10	92
3/2	3/2	0	184±3	223
5/2	5/2	0	304±2	296
7/2	7/2	0	337±2	337
9/2	9/2	0	364±2	359
11/2	11/2	0	364±5	370
5/2	5/2	−1	419±5	289
7/2	7/2	1	318±7	333
7/2	7/2	−1	351±10	333
9/2	9/2	−1	345±3	355
9/2	9/2	1	334±3	355
11/2	11/2	1	366±1	367
11/2	11/2	−1	369±1	367
7/2	7/2	2	161±1	319
9/2	9/2	−2	344±3	345
9/2	9/2	2	307±2	345
11/2	11/2	2	320±1	360
11/2	11/2	−2	492±1	360
9/2	9/2	−3	313±1	330

TABLE II. $T=1.7$ K, x-ray satellites associated with the $\left[\frac{1}{2}\ 0\ 0\right]$ displacement wave vector. Columns 2 and 3 show the experimental F_{exp}, and calculated F_{cal}, structure factors. F_{cal} is calculated for a relative displacement amplitude $\delta_{\langle 0\ 0\ \frac{1}{2}\rangle}/a=2.3\times10^{-3}$, assuming domains equipartition.

$(h\ k\ l)$			$F_{exp}(10^{-3}\ e^-)$	$F_{cal}(10^{-3}\ e^-)$
2	2	1/2	144±6	172
3	3	1/2	127±5	138
3	3	−1/2	122±5	138
4	4	1/2	127±5	114
4	4	−1/2	129±5	114
5	5	1/2	173±7	95
5	5	−1/2	149±6	95
3	3	−3/2	435±17	402
4	4	−3/2	297±12	334
5	5	3/2	251±10	281
5	5	−3/2	286±11	281
4	4	−5/2	463±18	533
5	5	5/2	373±15	453
5	5	−5/2	492±20	453
5	5	−7/2	795±32	608

TABLE III. $T=1.7$ K, x-ray satellites of the $\langle \frac{1}{4}\ \frac{1}{4}\ \frac{1}{2}\rangle$ type. The experimental F_{exp} and calculated F_{cal} structure factors are shown in columns 2 and 3, respectively. F_{cal} is calculated for a value of relative displacement amplitude $\delta_{\langle \frac{1}{4}\ \frac{1}{4}\ \frac{1}{2}\rangle}/a=1.9\times10^{-3}$, assuming domains equipartition.

$(h\ k\ l)$			$F_{exp}(10^{-3}\ e^-)$	$F_{cal}(10^{-3}\ e^-)$
7/4	7/4	1/2	173±5	106
9/4	9/4	1/2	72±2	94
9/4	9/4	−1/2	106±3	94
11/4	11/4	1/2	121±4	85
11/4	11/4	−1/2	103±3	85
13/4	13/4	1/2	84±3	76
13/4	13/4	−1/2	80±2	76
15/4	15/4	1/2	84±3	69
15/4	15/4	−1/2	82±3	69
17/4	17/4	1/2	72±2	63
17/4	17/4	−1/2	82±3	63
19/4	19/4	1/2	74±2	58
19/4	19/4	−1/2	50±2	58
13/4	13/4	3/2	132±4	222
13/4	13/4	−3/2	223±7	222
15/4	15/4	3/2	202±6	203
15/4	15/4	−3/2	189±6	203
17/4	17/4	3/2	147±5	185
17/4	17/4	−3/2	165±5	185
19/4	19/4	3/2	157±5	170
19/4	19/4	−3/2	167±5	170
21/4	21/4	3/2	145±4	157
21/4	21/4	−3/2	125±4	157
19/4	19/4	−5/2	294±9	273
21/4	21/4	5/2	188±6	253
21/4	21/4	−5/2	222±7	253

location of particular reflections, or for systematically carrying out large collections of intensities.

As the magnetic wave vectors belong to the $\langle \frac{1}{4}\ \frac{1}{4}\ \frac{1}{2}\rangle$ star, according to Eq. (9), the displacement wave vectors are expected to belong to the four following stars: $\langle \frac{1}{2}\ 0\ 0\rangle$, $\langle \frac{1}{2}\ \frac{1}{2}\ 0\rangle$, $\langle \frac{1}{4}\ \frac{1}{4}\ \frac{1}{2}\rangle$, and $\langle \frac{1}{4}\ \frac{1}{4}\ 0\rangle$. Two large collections of ω scans were thus performed at 1.7 and 12 K at the reciprocal space positions expected for these four types of displacement satellites. Particular attention was devoted to the specular reflections of the type $[(2n+1)/2\ (2n+1)/2\ 0]$. A collection of ten main Bragg reflections was also performed for the purposes of the normalization. Finally the thermal evolution of the integrated intensity of satellites representative of each family was followed from 1.7 K up to T_N.

For each reflection, the integrated intensity was corrected from the Lorentz $(L=1/\sin 2\theta_B)$ and polarization $(P=\cos^2 2\theta_B)$ factors. Off-specular reflections $(l\neq 0)$ were further corrected from the absorption factor $(A=2\sin(\theta_B-\varphi)/[\sin(\theta_B-\varphi)+\sin(\theta_B+\varphi)]$, φ being the angle between the surface and the reticular plane). Finally, a value of the

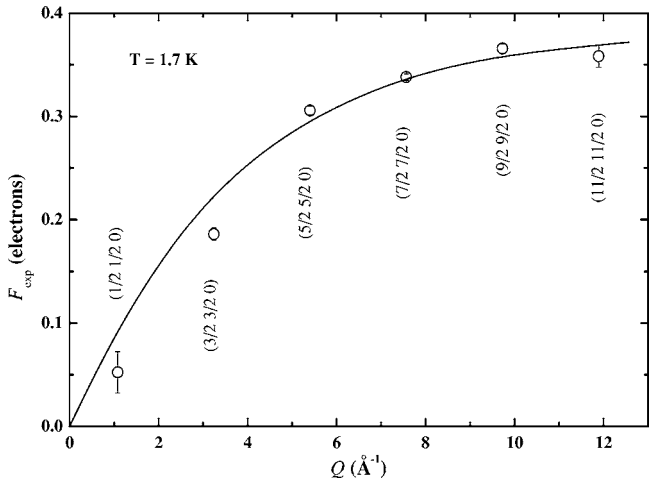

FIG. 3. Experimental structure factors (open circles) of the specular reflections of the $\langle \frac{1}{2}\ \frac{1}{2}\ 0\rangle$ type in GdB_6. The full line represents a computed structure factor, proportional to $f_{Gd}(Q)Q$.

experimental structure factor F_{exp}, in equivalent Thomson electrons, was derived from the normalized intensity. The reported experimental error results mainly from the definition of the background.

1. The low-temperature phase

At 1.7 K, in addition to the $\langle \frac{1}{2}\ 0\ 0\rangle$ and $\langle \frac{1}{2}\ \frac{1}{2}\ 0\rangle$ satellites already reported in Ref. 12, $\langle \frac{1}{4}\ \frac{1}{4}\ \frac{1}{2}\rangle$-type satellites are observed. Note that in the former experiments, no search was performed at these reciprocal space positions. The integrated intensities of all the measured satellites are reported in Tables I–III. As shown in Table III, the intensities of the $\langle \frac{1}{4}\ \frac{1}{4}\ \frac{1}{2}\rangle$-type satellites are of the same order of magnitude as the intensities of the $\langle \frac{1}{2}\ \frac{1}{2}\ 0\rangle$ or $\langle 0\ 0\ \frac{1}{2}\rangle$ satellites, much larger indeed than any possible magnetic reflection. This can be checked thanks to an estimate of the maximum, off-resonant, magnetic scattering amplitude[22] of Gd^{3+} for 18-keV incident photons. Considering optimal geometric conditions, a fully polarized magnetic ion, a small scattering angle, and domains equipartition, this scattering amplitude reaches 31×10^{-3} in equivalent Thomson electrons. This represents less than the smallest value of structure factor in Table III, which definitively rules out a magnetic origin for these satellites. Despite an extended search, no satellite could be detected at the reciprocal space positions associated with propagations of the $\langle \frac{1}{4}\ \frac{1}{4}\ 0\rangle$ star. According to Eq. (13b), this is consistent with a constant amplitude magnetic structure.

Figure 3 shows the experimental structure factor F_{exp} for all the observable specular reflections associated with the $\langle \frac{1}{2}\ \frac{1}{2}\ 0\rangle$ star. Contrary to the main charge reflections, F_{exp} tends to vanish as Q goes to zero. As shown by the solid line in Fig. 3, this variation is well accounted for by the product $f_{Gd}(Q)Q$, as expected for the atomic displacement wave structure factor [Eq. (24)]. This consistency attests that the domain distribution is essentially the same within the sample's volumes contributing to these specular reflections. In such conditions, for parallel scattering vectors, the factor $D(\boldsymbol{Q})$ in Eq. (24) is independent of $\boldsymbol{Q}$ and F_{exp} scales with the product $f_{Gd}(Q)Q$.

With an additional hypothesis of domain equipartition, the value of $D(\boldsymbol{Q})$ can be determined. Then, from Eq. (24), an estimate of the total $\langle \frac{1}{2}\ \frac{1}{2}\ 0\rangle$ displacement amplitude, $\delta_{\langle \frac{1}{2}\ \frac{1}{2}\ 0\rangle}$, can be derived from the experiment. After Eqs. (13), in the case of the $\left[\frac{1}{2}\ \frac{1}{2}\ 0\right]$ propagation, the displacements are within the plane defined by the directions of the half integer indexes. For the $(h\ h\ 0)$-type reflections observed here, Eq. (25) yields the value $\sqrt{1/6}$ for $D(\boldsymbol{Q})$. The value then deduced for the relative displacement amplitude is $\delta_{\langle \frac{1}{2}\ \frac{1}{2}\ 0\rangle}/a=(8.8\pm0.5)\times10^{-4}$. The discrepancies between calculation and experiment, observed in Fig. 3 at low Q, for the $\left(\frac{1}{2}\ \frac{1}{2}\ 0\right)$ and $\left(\frac{3}{2}\ \frac{3}{2}\ 0\right)$ reflections, may be ascribed to a slight variation of the $D(\boldsymbol{Q})$ factor. An alternative explanation is the interference of the scattering by a periodically distorted boron lattice. This contribution has been neglected in the present approach but, due to a boron scattering factor decreasing much faster with Q than the one of Gd^{3+}, it may be still significant at low Q.

For the nonspecular reflections, $D(\boldsymbol{Q})$ depends on the direction of $\boldsymbol{Q}$. In the case of the $\boldsymbol{Q}=(2\pi/a)[h\ h\ l]$ reflections measured in the present work and within the equipartition hypothesis, it can be expressed as

$$D(\boldsymbol{Q})=\sqrt{\frac{1}{6}}(1+l^2/2h^2)^{-\frac{1}{2}}.$$

In Table I are compared the experimental structure factor F_{exp} and the value F_{cal} calculated with a relative displacement amplitude $\delta_{\langle \frac{1}{2}\ \frac{1}{2}\ 0\rangle}/a$ of 8.8×10^{-4}. It can be noted that the experimental structure factors present some dispersions in comparison with the calculated values [see for instance the equivalent $(h\ h\ l)$ and $(h\ h\ -l)$ reflections]. Such a dispersion can be ascribed to the already mentioned imperfect orientation matrix, as an effect of the sample mosaic. It could also result from variations in the domains distribution through the $D(\boldsymbol{Q})$ factor.

Due to the experimental geometry, the reflections associated with the $\langle \frac{1}{2}\ 0\ 0\rangle$ and $\langle \frac{1}{4}\ \frac{1}{4}\ \frac{1}{2}\rangle$ stars are all off-specular. According to Eq. (13) the $\langle \frac{1}{2}\ 0\ 0\rangle$ displacement waves should be longitudinal. With the absence of $\langle \frac{1}{4}\ \frac{1}{4}\ 0\rangle$ satellites, it is justified to suppose a magnetic structure with constant amplitude. Then the $\langle \frac{1}{4}\ \frac{1}{4}\ \frac{1}{2}\rangle$ displacement waves are expected to be polarized along the direction of the one-half index. Within the hypothesis of domain equipartition, an estimate of the relative displacement amplitudes for these two wave vectors stars can be obtained. For the particular reflections of the $(h\ h\ l)$ type, measured here, the domain factors are

$$D(\boldsymbol{Q})=\sqrt{\frac{1}{3}}(1+2h^2/l^2)^{-\frac{1}{2}}\ \text{for}\ \boldsymbol{q}=\left[0\ 0\ \tfrac{1}{2}\right],$$

$$D(\boldsymbol{Q})=\sqrt{\frac{1}{6}}(1+2h^2/l^2)^{-\frac{1}{2}}\ \text{for}\ \boldsymbol{q}\in\langle \tfrac{1}{4}\ \tfrac{1}{4}\ \tfrac{1}{2}\rangle.$$

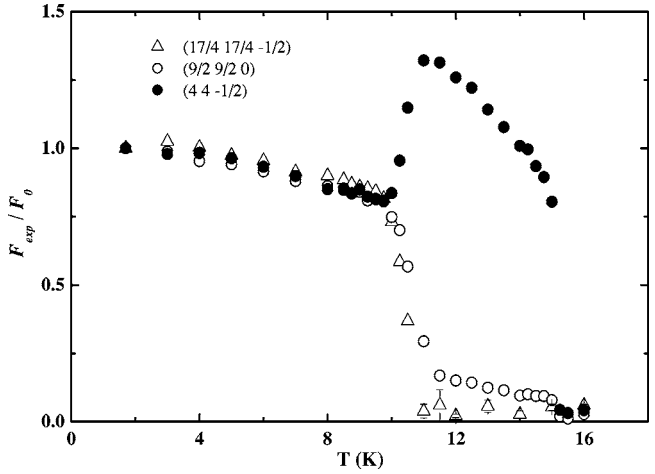

FIG. 4. Temperature dependence of the normalized, experimental, structure factor, F_{exp}/F_0, for three representative x-ray satellites in GdB_6. F_0 is the structure factor value at 1.7 K.

In Tables II and III are reported the experimental structure factors of all the observed reflections. They are compared with the first-order structure factors calculated according to the experimental determinations $\delta_{\langle 0\,0\,\frac{1}{2}\rangle}/a=(2.3\pm0.4)\times10^{-3}$ and $\delta_{\langle \frac{1}{4}\,\frac{1}{4}\,\frac{1}{2}\rangle}/a=(1.9\pm0.5)\times10^{-3}$. In spite of some discrepancies, the experimental data compare well with the calculated ones. These discrepancies, as for the nonspecular $\langle \frac{1}{2}\,\frac{1}{2}\,0\rangle$ reflections, can be ascribed to the crystal mosaic or to variations in the domains distribution.

The coexistence of three different types of displacement wave vectors bears evidence of the complexity of the displacement structure in this low-temperature phase. A reliable determination of this structure would require

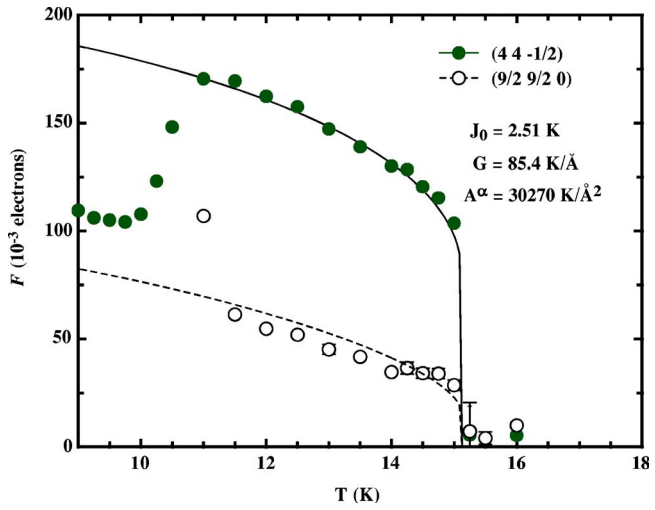

FIG. 5. (Color online) Detail of the thermal variation, in the high-temperature phase, for the $(4\ 4\ -\frac{1}{2})$ (full circles) and $(\frac{9}{2}\ \frac{9}{2}\ 0)$ (open circles) structure factors. The full and dashed lines represent the mean-field calculation for the $(4\ 4\ -\frac{1}{2})$ and $(\frac{9}{2}\ \frac{9}{2}\ 0)$ reflections, respectively, within the double-q displacement model (b) of Fig. 1 and for the values given in the figure.

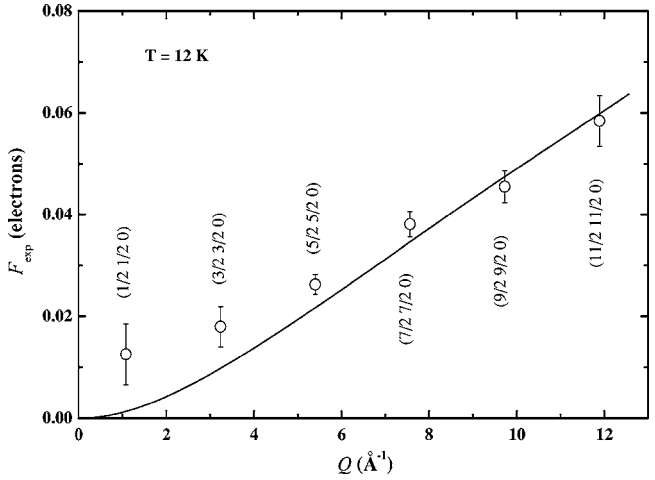

FIG. 6. Experimental structure factor F_{exp}, of the specular reflections of the $\langle \frac{1}{2}\,\frac{1}{2}\,0\rangle$ family at 12 K. The full line represents the calculated, second-order, structure factor which is proportional to $f_{\mathrm{Gd}}(Q)Q^2$.

(i) a better accuracy in the measurement of the intensities,

(ii) the question of the domain distribution to be addressed using an applied magnetic field (as for the determination of complex magnetic structures using neutron scattering on a single crystal).

In the present conditions, proposing a model of displacement structure for this phase would be hardly better than guessing.

2. Thermal variation

Figure 4 shows the thermal variation of the square root of the experimental integrated intensity F_{exp}, for three representative satellites: $(4\ 4\ -\frac{1}{2})$, $(\frac{9}{2}\ \frac{9}{2}\ 0)$, and $(\frac{17}{4}\ \frac{17}{4}\ -\frac{1}{2})$. These three reflections have been chosen because they have comparable values of Q. In the figure the experimental amplitude F_{exp} is normalized to its value F_0 at 1.7 K. Such a representation clearly shows the same thermal evolution in the low-temperature phase for the three satellites, thus confirming a same physical origin for all the reflections. Around 10 K, the sudden drop of the intensity of both the $(\frac{9}{2}\ \frac{9}{2}\ 0)$ and $(\frac{17}{4}\ \frac{17}{4}\ -\frac{1}{2})$ reflections is concomitant with the intensity increase of the $(4\ 4\ -\frac{1}{2})$ one. Raising the temperature up to 16 K, this last reflection passes through a maximum around 11 K before slowly decreasing. At T_N, its abrupt fall is coherent with the first-order transition. At 11.5 K, the $(\frac{17}{4}\ \frac{17}{4}\ -\frac{1}{2})$ reflection is no longer distinguishable from the background. On the contrary, the $(\frac{9}{2}\ \frac{9}{2}\ 0)$ one keeps an observable intensity up to T_N, where it abruptly drops. This is emphasized in Fig. 5, where the detail of the variation in the high-temperature phase is given for the $(\frac{9}{2}\ \frac{9}{2}\ 0)$ and $(4\ 4\ -\frac{1}{2})$ reflections. The observation of a well-resolved satellite of the $\langle \frac{1}{2}\,\frac{1}{2}\,0\rangle$ star in addition with those of the $\langle \frac{1}{2}\,0\,0\rangle$ type is an interesting feature, compared to the results in Ref. 12. It is worth noting that the experimental conditions of this previous work flux, Q resolution, and x-ray energy, made the observation of such weak intensities difficult. In the present one, besides the high per-

formance of the ESRF ID20 beamline, we took advantage of probing a larger volume of the sample using 18-keV incident x-rays. It can be pointed out, however, that the two reflections apparently present different thermal variations, that will be discussed later on.

3. The high-temperature phase

The data collection at 12 K confirms that the $\langle \frac{1}{4}\ \frac{1}{4}\ \frac{1}{2}\rangle$-type satellites are no longer observable. It is important to note that, unlike the x-ray diffraction, the powder neutron diffraction data[13] show no significant change in the magnitude of the $\langle \frac{1}{4}\ \frac{1}{4}\ \frac{1}{2}\rangle$ magnetic reflections at T^*. This confirms that the low temperature, $\langle \frac{1}{4}\ \frac{1}{4}\ \frac{1}{2}\rangle$, x-ray satellites cannot originate from magnetic scattering. As in the low-temperature phase, there are also no satellites associated with the $\langle \frac{1}{4}\ \frac{1}{4}\ 0\rangle$ star. The only present reflections are related to the $\langle \frac{1}{2}\ 0\ 0\rangle$ and $\langle \frac{1}{2}\ \frac{1}{2}\ 0\rangle$ stars. These latter are of much weaker intensity and their observation turns out to be of utmost importance. Figure 6 displays the experimental structure factor F_{exp} obtained at 12 K for the same set of $\langle \frac{1}{2}\ \frac{1}{2}\ 0\rangle$ specular reflections as the one of Fig. 3. At 12 K, its variation with Q is clearly different from the one at 1.7 K. The full line in Fig. 6 shows that this Q dependence agrees well with a scaled, $f_{\mathrm{Gd}}(Q)Q^2$, function. This is exactly what one expects from the second-order term of the scattering, according to Eq. (23). Except at low Q, particularly for the $(\frac{1}{2}\ \frac{1}{2}\ 0)$ reflection, the experimental data are well described by the $f_{\mathrm{Gd}}(Q)Q^2$ function. If it does not simply reflect local variations in the domain distribution, this discrepancy may be ascribed to a slight $\lambda/2$ contamination, the (1 1 0) reflection being one of the most intense charge reflections. The Q dependence of these $\langle \frac{1}{2}\ \frac{1}{2}\ 0\rangle$ reflections is then a strong evidence that they originate from a second-order scattering by the displacement waves. As the first-order scattering gives rise to the rather intense $\langle \frac{1}{2}\ 0\ 0\rangle$ reflections, the high-temperature displacement structure is of the $\langle \frac{1}{2}\ 0\ 0\rangle$ type. Moreover, the second-order $\langle \frac{1}{2}\ \frac{1}{2}\ 0\rangle$ satellites can emerge only if this structure is a multi-q one, the $\langle \frac{1}{2}\ \frac{1}{2}\ 0\rangle$ vectors resulting from the addition of separate members of the $\langle \frac{1}{2}\ 0\ 0\rangle$ star.

If one restricts to high-symmetry models of the displacement structures, that is, models for which all Gd ions are in (cubic) symmetry equivalent situations, there are very few multi-q, $\langle \frac{1}{2}\ 0\ 0\rangle$, solutions (analogous models of magnetic structures are discussed in Ref. 23). Only such high-symmetry solutions are consistent with a single-site treatment, then with the mean-field factorization of Sec. II C 1. Moreover, after Eq. (13), the polarization of the $\langle \frac{1}{2}\ 0\ 0\rangle$ displacement waves should be longitudinal. Finally, only two models of displacement structure may be considered:

(i) a triple-q, single domain, structure described by

$$\boldsymbol{q}_1 = \left[\tfrac{1}{2}\ 0\ 0\right] \text{ propagating } \boldsymbol{\delta}_1 = (1/\sqrt{3})[\delta\ 0\ 0],$$

$$\boldsymbol{q}_2 = \left[0\ \tfrac{1}{2}\ 0\right] \text{ propagating } \boldsymbol{\delta}_2 = (1/\sqrt{3})[0\ \delta\ 0],$$

$$\boldsymbol{q}_3 = \left[0\ 0\ \tfrac{1}{2}\right] \text{ propagating } \boldsymbol{\delta}_3 = (1/\sqrt{3})[0\ 0\ \delta],$$

(ii) a double-q, three domain, structure with domain Δ_{xy} described by

$$\boldsymbol{q}_1 = \left[\tfrac{1}{2}\ 0\ 0\right] \text{ propagating } \boldsymbol{\delta}_1 = (1/\sqrt{2})[\delta\ 0\ 0],$$

$$\boldsymbol{q}_2 = \left[0\ \tfrac{1}{2}\ 0\right] \text{ propagating } \boldsymbol{\delta}_2 = (1/\sqrt{2})[0\ \delta\ 0].$$

In both cases, δ represents the total amplitude of the displacement. Within the hypothesis of domain equipartition, these two models result in an identical form for the first-order structure factor that should describe the $\langle \frac{1}{2}\ 0\ 0\rangle$-type reflections. After Eq. (24), for the (hhl)-type reflections measured here, it reads as

$$F_{\mathrm{cal}}(\boldsymbol{Q}) = f_R(Q)Q\delta\frac{1}{\sqrt{3}}(1+2h^2/l^2)^{-\frac{1}{2}}.$$

The value of the relative displacement amplitude thus determined from the experiment is $\delta/a = (3.4 \pm 0.7) \times 10^{-3}$.

Considering now the specular reflections arising from the second-order mechanism, for the triple-q structure, only the propagations $\boldsymbol{q}_1$ and $\boldsymbol{q}_2$ contribute to the reflections through their sum $\left[\frac{1}{2}\ \frac{1}{2}\ 0\right]$. After Eq. (23), the structure factor describing the experimental data should be

$$F^{3q}_{\mathrm{cal}}(\boldsymbol{Q}) = f_R(Q)Q^2\frac{\delta^2}{6}.$$

For the double-q model, Δ_{xy} is the only domain contributing to the second-order reflections. Assuming domain equipartition, it represents one-third of the scattering volume and the calculated structure factor is

$$F^{2q}_{\mathrm{cal}}(\boldsymbol{Q}) = f_R(Q)Q^2\frac{\delta^2}{4\sqrt{3}}.$$

While the two models cannot be experimentally distinguished from the first-order reflections, it appears that the second-order ones could be selective. Indeed, the experimental value of relative displacement amplitude differ for the two models. Assuming a triple-q displacement structure, one obtains $\delta/a = (3.8 \pm 0.2) \times 10^{-3}$, whereas for the double-q models it becomes $\delta/a = (4.0 \pm 0.2) \times 10^{-3}$. Unfortunately, the difference between these two determinations does not exceed the experimental errors. Moreover, both are consistent with the first-order determination, $\delta/a = (3.4 \pm 0.7) \times 10^{-3}$, which does not help in choosing between the two models of displacement structures.

However, if one compares these two models with those which have been shown to minimize the exchange energy (see Fig. 1), the choice is quite obvious. Model (b) in Fig. 1 is precisely a double-q, $\langle \frac{1}{2}\ 0\ 0\rangle$, displacement structure. In Table IV are reported the experimental and calculated structure factors of the first- and second-order satellites [Eqs. (23) and (24)], assuming a double-q model with domain equipartition and a relative displacement amplitude $\delta/a = 3.9 \times 10^{-3}$. The agreement between the experimental and calculated structure factors is satisfactory for specular or close to specular reflections. For this collection again, the off-specular reflections show a significant dispersion related to

TABLE IV. $T=12$ K: second and fifth columns from left represent the experimental structure factor F_{exp} for the $\langle \frac{1}{2}\ 0\ 0 \rangle$- and $\langle \frac{1}{2}\ \frac{1}{2}\ 0 \rangle$-type satellites, respectively. The third and sixth columns give the calculated structure factors F_{cal} within the double-q model, with domain equipartition and a relative displacement amplitude $\delta/a=3.9\times10^{-3}$. The structure factors unit is 10^{-3} Thomson electron.

(hkl)			F_{exp}	F_{cal}	(hkl)			F_{exp}	F_{cal}
2	2	1/2	224±9	293	1/2	1/2	0	12.6±6	1
3	3	1/2	156±5	236	3/2	3/2	0	18±4	9
3	3	−1/2	165±7	236	5/2	5/2	0	26±2	20
4	4	1/2	165±6	194	7/2	7/2	0	38±2	32
4	4	−1/2	193±9	194	9/2	9/2	0	46±3	44
5	5	1/2	187±7	162	11/2	11/2	0	58±5	56
5	5	−1/2	172±7	162	5/2	5/2	−1	37±2	20
3	3	−3/2	552±22	685	7/2	7/2	1	39±1	32
4	4	−3/2	379±15	569	7/2	7/2	−1	42±1	32
5	5	3/2	293±12	478	7/2	7/2	−2	44±2	30
5	5	−3/2	332±13	478	9/2	9/2	−3	45±3	41
4	4	−5/2	601±24	907	9/2	9/2	−1	46±1	43
5	5	5/2	412±17	772	9/2	9/2	1	45±1	43
5	5	−5/2	653±26	772	9/2	9/2	−2	44±2	42
5	5	−7/2	896±36	1036	9/2	9/2	2	43±1	42
					11/2	11/2	2	57±6	54
					11/2	11/2	−2	58±7	54
					11/2	11/2	1	67±3	55
					11/2	11/2	−1	71±3	55

the mosaic spread and/or variations in the domains distribution.

Finally, the consistency of the mean-field model of Sec. II A can be tested through the thermal variations of the reflections $(4\ 4\ -\frac{1}{2})$ and $(\frac{9}{2}\ \frac{9}{2}\ 0)$. In practical terms, at a given temperature, self-consistent calculations based on the mean-field expression of Eq. (18), for a Brillouin-type response of Gd^{3+}, provide the statistical value of the ordered magnetic moment. Then, in the context of model (b) (Fig. 1), the displacement is deduced after Eqs. (13). Finally, within the hypothesis of domains equipartition, the structure factors for reflections $(4\ 4\ -\frac{1}{2})$ and $(\frac{9}{2}\ \frac{9}{2}\ 0)$ can be computed. The values that are so obtained depend on three adjustable parameters: the exchange coupling constant J_0, the harmonic potential constant A^{α}, and the coupling gradient factor G. As shown in Fig. 5, the thermal variation of the structure factors is well reproduced with the set $J_0=2.51$ K, $A^{\alpha}=30\,270$ K/Å^2, and $G=85.4$ K/Å. The calculated transition at T_N has a strong first-order character. Indeed, if the only magnetic exchange is taken into account, a value of 2.51 K for J_0 would lead to a second-order transition at a temperature of 13.1 K, instead of the present 15.1 K. However, this set of parameters has to be taken with caution since it depends largely on the assumption of domains equipartition.

IV. CONCLUSION

This x-ray experimental study of GdB_6 has confirmed that the satellite reflections appearing below T_N are due to atomic displacement waves. Their dependence on the scattering angle is typical of such a phenomenon and consistent with movements of the Gd ions only, with negligible interference of the boron lattice. The amplitude of the displacement is sufficient for allowing the observation of second-order diffraction peaks; that is, the scattering by a wave representing the square of the atomic displacements. In the case of GdB_6 high-temperature antiferromagnetic phase, the emergence of second-order satellites provides a direct evidence for the multiaxial character of the displacement structure. The only first-order reflections in this phase are characteristic of $\langle \frac{1}{2}\ 0\ 0 \rangle$ waves, whereas the second order are of the $\langle \frac{1}{2}\ \frac{1}{2}\ 0 \rangle$ type which result from the addition of different members of the $\langle \frac{1}{2}\ 0\ 0 \rangle$ star. The high-temperature displacement structure of GdB_6 is then multi q, which is consistent with only two multiaxial high-symmetry models; double q or triple q.

In the low-temperature phase, first-order reflections arising from $\langle \frac{1}{4}\ \frac{1}{4}\ \frac{1}{2} \rangle$, $\langle \frac{1}{2}\ 0\ 0 \rangle$, and $\langle \frac{1}{2}\ \frac{1}{2}\ 0 \rangle$ displacement waves are observed. This indicates a more complex displacement scheme than in the high-temperature antiferromagnetic phase; the unavoidable problem of domains (in zero applied field), together with the difficulties in relying quantitatively on a large set of reflections, leave the determination of this second displacement structure incomplete.

The x-ray data are consistent with the mean-field model introduced here, at least with regard to the relation between magnetic and displacement wave vectors. For a given magnetic structure, this model defines the associated displacement waves, in terms of wave vectors and polarization. This

latter reflects the symmetry of the lattice and, eventually, determines the direction of the displacement.

This model also shows that the interference of the displacement is equivalent to the emergence of fourth-order terms in the magnetic energy of the system, similarly to the effect of biquadratic couplings. It follows that they can determine a transition of the first order at T_N and lift the degeneracy between the various magnetic models based on a same wave vectors star. In the $\langle \frac{1}{4}\ \frac{1}{4}\ \frac{1}{2} \rangle$ magnetic case investigated here, the analysis, confined to planar models, shows that two collinear models are equally privileged by the displacements. One corresponds to a uniaxial, $\langle \frac{1}{2}\ \frac{1}{2}\ 0 \rangle$, displacement structure, whereas the other is a double q, $\langle \frac{1}{2}\ 0\ 0 \rangle$, then a biaxial structure. This latter is the only one consistent with the x-ray-diffraction results in the high-temperature phase; its $\langle \frac{1}{2}\ 0\ 0 \rangle$ wave vectors correspond to the first-order reflections and its double-q character accounts for the observation of $\langle \frac{1}{2}\ \frac{1}{2}\ 0 \rangle$ second-order satellites. Moreover, the collinear nature of this magnetic model explains the high, essentially isotropic, magnetic susceptibility of this antiferromagnetic phase.[24] In this case, the joint use of x-ray data and of the analytical relation between magnetic and displacement structures leaves little uncertainty about the nature of this ordered state. However, this approach does not account for the existence of a second, low-temperature, phase whose displacement structure cannot be identified with one of the two, exchange privileged, models.

At this point, one is apparently faced with the limitations of a modeling based only on isotropic exchange and magnetic ions moving in a harmonic potential. Indeed, such ingredients are unlikely to result in a change of the ordered state within the narrow temperature range of GdB_6 antiferromagnetism. If a transition occurs, a competition between energy terms with different temperature dependencies is to be invoked. The best candidate for introducing such an effect is the anisotropy affecting the displacement of the ions in their cubic environment. Indeed, in the model we used, the second-order potential, in which the Gd ions move, forbids any anisotropy. Obviously, as the displacement amplitude increases, neglecting higher-order terms in this potential becomes questionable. The next terms to appear are of the fourth order which, for a cubic symmetry, means an anisotropy in favor of fourfold or threefold displacement axes. These two kinds of easy-displacement axes are then in contradiction with the twofold ones of the structure selected for the high-temperature phase. Close to T_N, this phase is well described by the model restricted to the harmonic well but, as the temperature decreases and the displacement amplitude increases, the conflict with the displacement anisotropy is inevitable. This can explain the transition at T^*; to lower its anisotropy energy, the system adopts another magnetic structure whose associated displacement axes better comply with the anisotropy. Confirming this scenario requires additional x-ray experiments under an applied field to deal with the domain's partition.

Nevertheless, this study of GdB_6 antiferromagnetic range is a different illustration of the influence of magnetoelastic phenomena on the ordering properties of rare-earth compounds. In GdB_6, they take the original form of static displacement waves which concomitantly develop with the magnetic order. In case of a noncentrosymmetric magnetic wave vector, moving the magnetic ions with respect to their paramagnetic equilibrium position can decrease the exchange energy. Such a mechanism is particularly influential in the context of isotropic couplings between S-type ions on a cubic lattice, favorable for degeneracy. In GdB_6, the present study has shown that it has indeed a determining effect on the nature and thermodynamics of the ordered states. Except for a particular crystallography, which gives the displacement an unusual amplitude, the involved ingredients are not specific to GdB_6. An influence of displacement waves is then to be expected in many other gadolinium intermetallic compounds.

In $L \neq 0$ cubic systems, exchange induced displacements should also take place in the magnetic order range. Their effects will be mixed with those related to the orbital degeneracy and the relative influence of the two mechanisms will be quite difficult to analyze. Anyway, they should not be considered independently since a displacement lowers the cubic symmetry and, inevitably, results in the emergence of quadrupolar components.

*Electronic address: amara@grenoble.cnrs.fr

[1] H. Bethe, Ann. Phys. **3**, 133 (1929).
[2] K. Lea, M. Leask, and W. Wolf, J. Phys. Chem. Solids **23**, 1381 (1962).
[3] D. Schmitt, J. Phys. (France) **47**, 677 (1986).
[4] P. Morin and D. Schmitt, *Quadrupolar Interactions and Magnetoelastic Effects in Rare Earth Intermetallic Compounds*, Ferromagnetic Materials, No. 5 (Elsevier Science, New York, 1990), Chap. 1, p. 1.
[5] R. Aléonard, P. Morin, J. Pierre, and D. Schmitt, Solid State Commun. **17**, 599 (1975).
[6] D. Kim and P.-M. Levy, J. Magn. Magn. Mater. **27**, 257 (1982).
[7] C. Bean and D. Rodbell, Phys. Rev. **126**, 104 (1962).
[8] M. Lines and E. Jones, Phys. Rev. **139**, A1313 (1965).
[9] J. Pierre and B. Hennion, *Crystalline Electric Field and Structural Effects in f-Electron Systems* (Plenum, New York, 1982), p. 275.
[10] H. Hacker, Y. Shimada, and K. S. Chung, Phys. Status Solidi A **4**, 459 (1971).
[11] H. Nozaki, T. Tanaka, and Y. Ishizawa, J. Phys. C **13**, 2751 (1980).
[12] R.-M. Galéra, D.-P. Osterman, and J.-D. Axe, J. Appl. Phys. **63**, 3580 (1988).
[13] S. Luca, M. Amara, R.-M. Galéra, F. Givord, S. Granovsky, O. Isnard, and B. Beuneu, Physica B **350**, e39 (2004).
[14] T. Kasuya, J. Magn. Magn. Mater. **174**, L28 (1997).
[15] I. A. Zaliznyak, Phys. Rev. B **68**, 134451 (2003).
[16] P.-G. de Gennes, C. R. Hebd. Seances Acad. Sci. **247**, 1836

(1958).
[17] G. Uimin, Phys. Rev. B **55**, 8267 (1997).
[18] T. Kasuya, J. Phys. Soc. Jpn. **67**, 33 (1998).
[19] K. Segawa, A. Tomita, K. Iwashita, M. Kasaya, T. Suzuki, and S. Kunii, J. Magn. Magn. Mater. **104-107**, 1233 (1992).
[20] K. Takahashi, H. Nojiri, K. Ohoyama, M. Ohashi, Y. Yamaguchi, M. Motokawa, and S. Kunii, J. Magn. Magn. Mater. **177-181**, 1097 (1998).
[21] S. Kunii, K. Takeuchi, I. Oguro, K. Sugiyama, A. Ohya, M. Yamada, Y. Koyoshi, M. Date, and T. Kasuya, J. Magn. Magn. Mater. **52**, 2751 (1985).
[22] M. Blume, J. Appl. Phys. **57**, 3615 (1985).
[23] M. Amara and P. Morin, Physica B **205**, 379 (1995).
[24] S. Luca, Ph.D. thesis, Université Joseph-Fourier, Grenoble, 2002, URL http://tel.ccsd.cnrs.fr/